LANGMUIR

pubs.acs.org/Langmuir Article

Flocculation of MXenes and Their Use as 2D Particle Surfactants for Capsule Formation

Huaixuan Cao,[†] Maria Escamilla,[†] Kailash Dhondiram Arole, Dustin Holta, Jodie L. Lutkenhaus, Miladin Radovic, Micah J. Green,* and Emily B. Pentzer*

Cite This: *Langmuir* 2021, 37, 2649–2657 Read Online

ACCESS | Metrics & More | Article Recommendations | Supporting Information

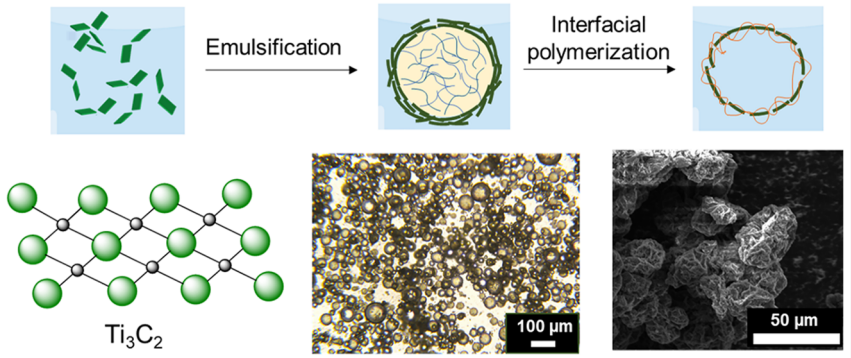

ABSTRACT: MXenes, transition metal carbides or nitrides, have gained great attention in recent years due to their high electrical conductivity and catalytic activity, hydrophilicity, and diverse surface chemistry. However, high hydrophilicity and negative ζ potential of the MXene nanosheets limit their processability and interfacial assembly. Previous examples for modifying the dispersibility and wettability of MXenes have focused on the use of organic ligands, such as alkyl amines, or covalent modification with triethoxysilanes. Here, we report a simple method to access MXene-stabilized oil-in-water emulsions by using common inorganic salts (e.g., NaCl) to flocculate the nanosheets and demonstrate the use of these Pickering emulsions to prepare capsules with shells of MXene and polymer. $Ti_3C_2T_z$ nanosheets are used as the representative MXene. The salt-flocculated MXene nanosheets produce emulsions that are stable for days, as determined by optical microscopy imaging. The incorporation of a diisocyanate in the discontinuous oil phase and diamine in the continuous water phase led to interfacial polymerization and the formation of capsules. The capsules were characterized by Fourier transform infrared (FTIR) spectroscopy, X-ray photoelectron spectroscopy (XPS), and scanning electron microscopy (SEM), confirming the presence of both polymer and nanosheets. The addition of ethanol to the capsules led to the removal of the toluene core and retention of the shell structure. The ability to assemble MXene nanosheets at fluid−fluid interfaces without the use of ligands or cosurfactants expands the accessible material constructs relevant for biomedical engineering, water purification, energy storage, electromagnetic electronics, catalysis, and so on.

INTRODUCTION

Emulsions are mixtures of two or more immiscible liquids, such as oil and water, where droplets of one liquid are dispersed in a continuous phase of the other. Commonly, amphiphilic small molecules or polymers are used as surfactants to stabilize emulsions; for example, sodium dodecyl sulfate (SDS) decreases the interfacial tension in oil-in-water emulsions by residing at the fluid−fluid interface with the alkyl chain exposed to the oil and the charged headgroup in the water. Molecular and polymeric surfactants have been used in the food, medicine, and cosmetics industries, among others. Alternatively, Pickering emulsions are those that are stabilized by solid particle surfactants and have gained much attention in emulsion technology.[1−4] Particle surfactants yield more stable emulsions than those that use small molecules, given the greater energy required to remove a particle from the fluid−fluid interface. Further, particle surfactants can lead to lower toxicity and a less negative environmental impact compared to some small molecule surfactants, and the multifunctional properties of the particles can be leveraged for additional applications (e.g., redox activity used for catalysis). Pickering emulsions have also had increased attention for use as templates to architect composite structures. For example, dispersion polymerization in Pickering emulsions can be used

Received: November 12, 2020
Revised: January 27, 2021
Published: February 16, 2021

https://dx.doi.org/10.1021/acs.langmuir.0c03244
Langmuir 2021, 37, 2649−2657

to prepare composite particles that can be processed into composite thin films above the T_g of the polymer.[5,6]

Spherical particles are typically used as Pickering surfactants, but there is growing interest in 2D particles (e.g., clay platelets and graphene oxide nanosheets). 2D particle surfactants are distinct in that their high aspect ratio leads to the particles being arranged parallel to the fluid−fluid interface, and therefore, a single particle covers significantly more area than its spherical counterpart. Pickering emulsions stabilized by 2D particles have been used as templates to fabricate Janus nanosheets, armored polymer particles, and capsules.[7−10] These systems make use of the spatial confinement of reagents enabled by the emulsion structure. For example, if one difunctional monomer is in the discontinuous phase and a complementary multifunctional monomer is in the continuous phase, interfacial polymerization gives a composite shell of polymer and nanosheet. Complementary approaches to capsule formation in Pickering emulsions include layer-by-layer assembly onto droplets, freeze-drying and annealing of emulsions, growth of an inorganic shell templated by droplets, deposition of a polymer onto droplets, and aerosol spray pyrolysis.[11−15] Our group has recently demonstrated that Pickering emulsions stabilized by graphene oxide (GO) nanosheets or their alkylated derivatives can be used to architect a number of structures and compositions. In these examples, the GO nanosheets only serve as the particle surfactant, and the properties of GO are not leveraged for performance in the final product.[16,17] The question remains as to whether MXenes might also be leveraged as sole surfactants in Pickering emulsions, enabling the preparation of composite architectures, which integrate the nanosheet properties.

MXene nanosheets are a relatively new class of 2D particles that possess high electrical conductivity and catalytic activity and distinct surface functionality.[18,19] MXenes are transition metal carbides or nitrides that have the general chemical formula of $M_{n+1}X_nT_z$ (n = 1−3), where M represents an early transition metal such as Ti or V; X is C or N; T_z represents the different functional groups on the surface (−O, −F, −OH).[20−22] MXene nanosheets are synthesized from a MAX phase by selectively etching a group "A" element (e.g., Al), giving a MAX clay that is then subjected to an exfoliation process.[23] The surface functionalities of MXene nanosheets render them hydrophilic and colloidally stable as aqueous dispersions. Typical ζ potentials for stable MXene dispersions at neutral pH are −30 to −40 mV. As aqueous dispersions, MXenes tend to oxidize into transition metal oxide (e.g., Ti_3C_2 oxidizes to TiO_2 after a few days); however, the addition of ascorbic acid or storage in the solid state can slow these changes.[24]

Recent research addresses the intercalation of MXene clays with small molecules to control interlayer spacing, the introduction of ions, or the formation of composites with other nanomaterials and polymers.[25−36] MXenes and their composites have a number of demonstrated applications in energy conversion and storage, water purification, biomedical engineering, electromagnetic shielding electronics, and catalysis.[37−45] One route to architecting composite structures is leveraging the interfacial assembly of MXene nanosheets in Pickering emulsions. All previous reports have made use of cosurfactants or ligands to facilitate the interfacial assembly of MXenes in oil-in-water emulsions. For example, Huang and co-workers added the well-known organic salt cetyltrimethylammonium bromide (CTAB) to an aqueous dispersion of Ti_3C_2 MXenes to form a dodecane-in-water emulsion; the ability to form emulsions was pH dependent, attributed to electrostatic interactions between the ammonium cation and negatively charged MXene surface.[46] Shi et al. combined an amine-terminated polyoctahedral silsesquioxane (POSS-NH_2) with Ti_3C_2 nanosheets to produce water-in-toluene Pickering emulsions, which were then concentrated and freeze-dried to obtain aerogels.[47] Alternatively, *n*-butylamine was used as a ligand/cosurfactant to fix MXene nanosheets at the toluene−water interface; this assembly was used to fabricate MXene thin films and liquid inks for printing in a matrix of silicone oil.[48] Yu and co-workers prepared Janus MXene nanosheets by electrostatically binding positively charged polystyrene to the negatively charged surface of the MXenes; the nanosheets stabilized toluene-in-water emulsions that were then used to produce aerogels and thin films.[49] In these systems, an organic cosurfactant is required for the assembly of MXene nanosheets at fluid−fluid interfaces, and this cosurfactant invariably becomes an integral part of the emulsion structure.

Here, we report a simple method to stabilize Pickering emulsions with $Ti_3C_2T_z$ MXenes by flocculating an aqueous dispersion of the nanosheets with an inorganic salt and use the emulsions to template capsule formation, giving a composite shell of polymer and nanosheet. Inorganic salts are selected as a flocculant because of prior success in the flocculation of clay nanosheets under these conditions. For example, Ashby and Binks demonstrated the importance of salts when flocculating the Laponite clay particles for the formation of oil-in-water emulsion.[50] Further, MXene gels have been prepared using multivalent salts, demonstrating the favorable salt/MXene interactions.[51] To prepare stable oil-in-water Pickering emulsions, MXene nanosheets are flocculated with NaCl; then, toluene is added, and the system is agitated. We examine the impact of the concentration and identity of the salt, as well as the concentration of MXenes, on the formation and stability of emulsion droplets, as characterized by optical microscopy imaging. Capsules are prepared by incorporating a diisocyanate in the toluene phase and diamine in the water phase such that interfacial polymerization produces a shell of MXene nanosheet and polyurea around the inner toluene core. The toluene core can be extracted by the addition of ethanol, leaving the shell intact, but collapsed. This is in direct contrast to the addition of ethanol to the emulsions themselves, which leads to the dispersion of the nanosheets. This work demonstrates, for the first time, the interfacial assembly of MXene nanosheets without organic small molecule or polymer cosurfactant, giving access to nonorganic surfactant compositions. This methodology may be used to produce novel MXene-based architectures with tailorable composition and applications in, e.g., energy storage and catalysis.[16,52]

MATERIALS AND METHODS

Materials. The Ti_3AlC_2 MAX phase was prepared as previously reported.[24,53] Lithium fluoride (LiF; 98%+) was purchased from Alfa Aesar. Hydrochloric acid (HCl; 37% [w/w], ACS reagent), dimethyl sulfoxide (DMSO; >99.5%), ethylenediamine (>99%), and hexamethylene diisocyanate (99%) were purchased from Sigma-Aldrich. All reagents were used as received without further purification.

Instrumentation. Emulsions were made using a hand-held emulsifier from BioSpec Products Inc. (model 985370). Optical microscopy images were obtained using an Amscope microscope. The samples were prepared by placing a drop of emulsion solution onto a glass slide. X-ray photoelectron spectroscopy (XPS) was performed using an Omicron X-ray photoelectron spectrometer employing a Mg-

https://dx.doi.org/10.1021/acs.langmuir.0c03244
Langmuir 2021, 37, 2649−2657

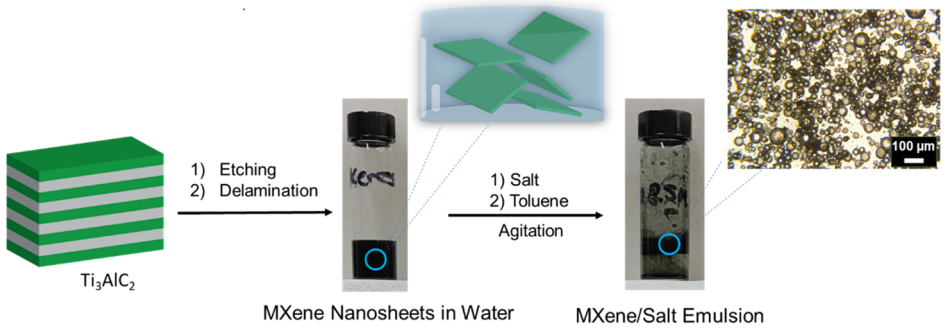

Figure 1. Preparation of $Ti_3C_2T_z$ nanosheets from the Ti_3AlC_2 MAX phase and their dispersion in water; salt flocculated $Ti_3C_2T_z$ nanosheets stabilized toluene-in-water Pickering type emulsions (1 mg/mL $Ti_3C_2T_z$ in water; 0.025 M NaCl; 1:5 vol/vol oil/water).

sourced X-ray beam at 15 kV with an aperture of 5. ζ potential and dynamic light scattering (DLS) measurements were performed using Zetasizer Nano ZS90 from Malvern Instruments and the appropriate capillary cell, DTS 1070, from Malvern Instruments; MXene nanosheet dispersions in water were diluted to 0.033 mg/mL prior to characterization. Transmission electron microscopy (TEM) was performed on an FEI Tecnai F20 transmission electron microscope operating at 200 kV. Scanning electron microscopy (SEM) was conducted on an FEI Quanta 600 field-emission scanning electron microscope with an acceleration voltage of 5 and 20 kV for microscopy and energy-dispersive X-ray spectroscopy (EDS) imaging, respectively. Fourier transform infrared (FTIR) spectra were collected on a JASCO FT/IR-4600 using 16 scans in ATR mode using a ZnSe/diamond prism.

Preparation of $Ti_3C_2T_z$ MXene Nanosheets. $Ti_3C_2T_z$ MXene nanosheets were synthesized following our previous work.[54] Briefly, 1.6 g of LiF was dissolved in 20 mL of 6 M aqueous HCl; then, 2 g of MAX powder was added to this solution. The mixture was stirred continuously at 40 °C for 40 h. The resulting suspension was centrifuged, and the supernatant was discarded. The precipitate ($Ti_3C_2T_z$ clay) was washed with deionized water until the water effluent reached a pH of ~6 as determined by litmus paper. The $Ti_3C_2T_z$ clay was intercalated with DMSO at room temperature for 20 h with continuous stirring. Then, excess DMSO was removed by washing 3 times with deionized water (dispersed in water and then centrifuged at 9000 rpm for 26 min; the supernatant was discarded, and then, fresh water was added, followed by a bath sonication for 1 h). To collect $Ti_3C_2T_z$ MXene nanosheets, the suspension was centrifuged at 3500 rpm for 45 min and the supernatant was collected.

Flocculation of MXene Nanosheets and Preparation of Emulsions. MXene/salt solutions were made with a MXene concentration of 1 or 3 mg/mL and salt concentrations of 0.005, 0.025, 0.05, and 0.1 M. For example, to prepare the 0.1 M NaCl solution of 1 mg/mL MXenes, 1 mL of MXene nanosheets (2 mg/mL) was added to glass vials; then, 1 mL of aqueous inorganic salt (0.2 M) was added. The vial was shaken vigorously by hand, and visible flocs were formed. To prepare the emulsions, toluene (0.4 mL) was added to the flocculated nanosheet suspension and the mixture was emulsified using a hand-held emulsifier at maximum agitation for a total of 60 s (3 × 20 s of agitation with 5 s pauses between).

Preparation of Capsules in Oil/Water Emulsions. Capsules were synthesized by interfacial polymerization in a Pickering emulsion stabilized by flocculated $Ti_3C_2T_z$ nanosheets. The aqueous phase was prepared by mixing an aqueous dispersion of $Ti_3C_2T_z$ MXenes (2 mg/mL, 1 mL) and NaCl (0.05 M, 1 mL) to give a concentration of 1 mg/mL MXenes, and the oil phase was prepared by dissolving hexamethylene diisocyanate (HDI) (0.5 mmol) in toluene (0.4 mL). The aqueous and oil phases were combined in a glass vial and agitated as described above. After emulsification, an aqueous solution of EDA (0.7 mmol EDA in 0.5 mL deionized water) was added to the continuous water phase, and the vial was swirled by hand. The mixture was stored at 4 °C for 72 h before quenching with ammonium hydroxide (30 wt %, 2 mL) in deionized water (40 mL). The capsules were obtained by gravity filtration and washed with water and then methanol. The isolated capsules were dried under reduced pressure at 20 °C and stored under vacuum (to prevent oxidation of MXenes).

Alcohol Challenge. Ethanol was added to both a sample of the emulsion and a sample of the capsules (before isolation). To test the stability, ethanol (3 mL) was added to the emulsion precursor prior to capsule formation (MXene nanosheets had been flocculated with NaCl, and the discontinuous phase was composed of HDI/toluene); after the addition of ethanol, the vial was shaken by hand and vortexed for 10 s. To test the stability of the capsules, ethanol (3 mL) was added to an aqueous dispersion of capsules (i.e., before isolation by filtration); then, the vial was shaken by hand and vortexed for 10 s. For each sample, a drop of the solution was placed on a glass slide and examined by optical microscopy.

RESULTS AND DISCUSSION

Preparation and Characterization of $Ti_3C_2T_z$ MXenes. $Ti_3C_2T_z$ MXenes were prepared and characterized as previously reported.[24,54] Briefly, etching Al from the Ti_3AlC_2MAX powder was completed using an aqueous LiF/HCl solution, followed by intercalation with DMSO and exfoliation. The resulting $Ti_3C_2T_z$ MXene nanosheets easily dispersed in water to give a transparent, dark green dispersion. The lateral size of the nanosheets ranged from hundreds of nanometers to a few micrometers (TEM images are shown in Figure S1). The dynamic light scattering measurements showed the average hydrodynamic diameter of the nanosheets was 360 nm. The ζ potential of the nanosheets was −46 mV (Table S1). This surface charge indicates a stable colloidal dispersion in water due to electrostatic repulsion between the nanosheets.

MXene-Stabilized Emulsions. Figure 1 shows the approach for the preparation of aqueous dispersions of MXene nanosheets, their flocculation, and their use to stabilize Pickering emulsions. We first tested whether $Ti_3C_2T_z$ nanosheets themselves could stabilize oil-in-water emulsions. Toluene and an aqueous dispersion of the nanosheets were agitated (1 mg/mL of nanosheets with 1:5 vol/vol oil/water); these are similar to the conditions used to prepare GO-stabilized emulsions. An emulsion was initially observed, as verified by optical microscopy imaging; however, the droplets disappeared, and macrophase separation of the oil and water was observed after only 2 h (Figure S2). On the basis of the highly hydrophilic nature of the nanosheets, these results were not surprising. We hypothesized that the addition of inorganic salts to the $Ti_3C_2T_z$ nanosheet solution would shield the negative charges on the nanosheet surfaces, resulting in their flocculation. This route is similar to that used for the interfacial

https://dx.doi.org/10.1021/acs.langmuir.0c03244
Langmuir 2021, 37, 2649−2657

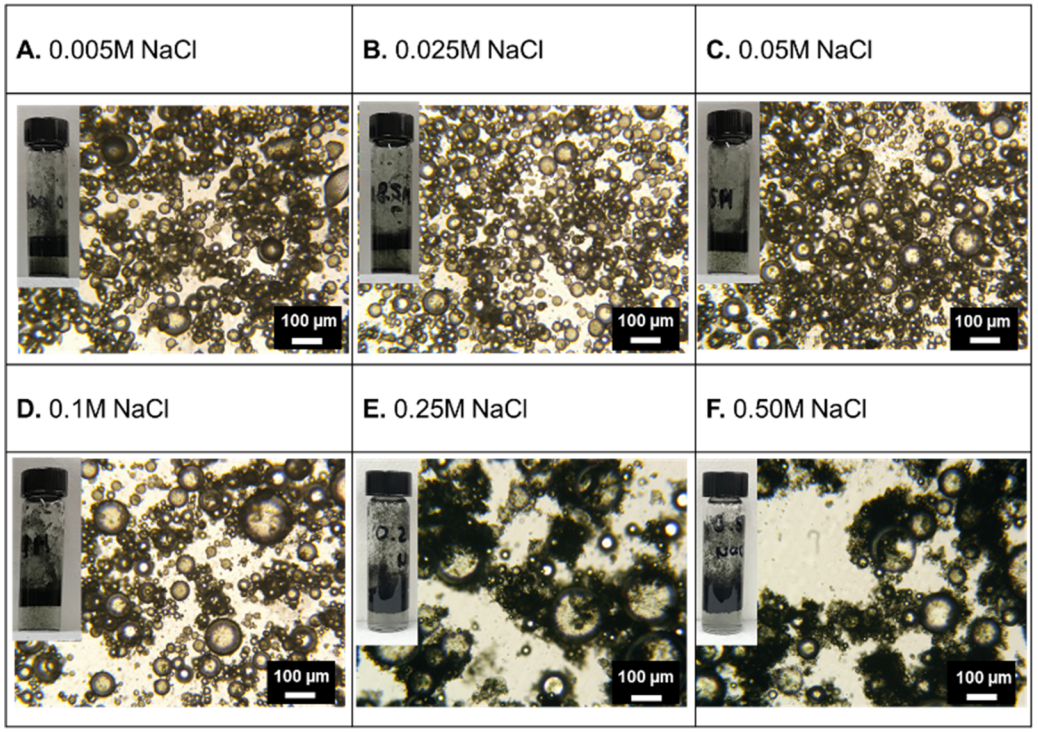

Figure 2. Optical microscopy images and photographs of 1:5 vol/vol toluene/water emulsions stabilized by 1 mg/mL $Ti_3C_2T_z$ nanosheets flocculated using NaCl concentrations of (A) 0.005 M, (B) 0.025 M, (C) 0.05 M, (D) 0.1 M, (E) 0.25 M, and (F) 0.5 M. Images were taken immediately after emulsion formation.

assembly of clay platelets (e.g., Montmorillonite) and in contrast to Pickering emulsions stabilized by GO nanosheets, which possess negative charge only at the nanosheet edges (i.e., faces of the nanosheet are neutral) and can form stable emulsions without the addition of salt. Of note, low salt concentrations also decrease the surface charge at the oil/water interfaces,[55] which may further facilitate nanosheet assembly at the interface and Pickering emulsion formation. At a NaCl concentration of 0.025 M, agitation of the biphasic mixture led to the formation of MXene-stabilized oil-in-water emulsions (Figure 1).

To determine the conditions that would produce stable and uniform emulsion droplets, five different NaCl concentrations (0.005, 0.025, 0.05, 0.1, and 0.5 M) and two different $Ti_3C_2T_z$ nanosheet concentrations (1 and 3 mg/mL) were investigated. Figure S3 shows the optical microscopy images of emulsions prepared with 3 mg/mL $Ti_3C_2T_z$; a wide range of droplet sizes are present, and the dark background indicates the presence of excess nanosheets in the continuous phase. In contrast, the optical microscopy images of emulsions stabilized by 1 mg/mL $Ti_3C_2T_z$, shown in Figure 2, reveal these emulsion droplets have well-defined shapes, and the continuous phase is light in color, indicating all nanosheets are present at the fluid−fluid interface. The comparison of the optical microscopy images of emulsions prepared with different concentrations of NaCl illustrates that larger, less-uniform droplets are formed as the concentration of salt is increased (i.e., compare Figure 2A−F). The less uniform droplets are also accompanied by darker regions, suggestive of large aggregates of $Ti_3C_2T_z$ nanosheets (compare Figure 2E,F). These images suggest that higher salt concentrations produce large aggregates of nanosheets that do not participate in the stabilization of the emulsion. After the emulsions were left to stand unagitated for 72 h, optical microscopy images were again taken (Figure S4); these images showed droplets of a similar size to those present immediately after emulsion formation. The most consistent and uniform size distribution of the droplets was obtained using a 1 mg/mL $Ti_3C_2T_z$ concentration and 0.025 M NaCl, as determined by the optical microscopy images.

We initially hypothesized that the addition of salt leads to an increase in ζ potential of the nanosheets (i.e., makes them less negatively charged). Therefore, the ζ potential of the $Ti_3C_2T_z$ nanosheet dispersions at different NaCl concentrations was compared; there was an increase of ζ potential from −46 to −14.1 mV at NaCl concentrations from 0 to 0.5 M (Table S1). Over this salt concentration range, no substantial change of solution pH was observed. Perhaps surprisingly, at the lowest salt concentrations tested (0.005 M NaCl), the ζ potential of the nanosheets decreased compared to the salt-free sample; this may be attributed to the chloride anions interacting with the positively charged nanosheet edges. A further increase in the salt concentration led to less negative ζ potential, as expected. Thus, the ability to form emulsions by the flocculation of MXenes with at an appropriate concentration of salt can be attributed to shielding of charges between the nanosheets and not directly related to ζ potential values. Of note, attempts to prepare water-in-oil emulsions using an excess of oil were not successful.

Three other inorganic salts were evaluated as flocculating agents for $Ti_3C_2T_z$ nanosheets and emulsion formation: LiCl, CsCl, and $MgCl_2$. The optimized conditions for NaCl were initially used (1 mg/mL $Ti_3C_2T_z$ and 0.025 M salt). Figure 3 shows representative optical microscopy images of the resulting emulsions, indicating that only CsCl led to the formation of uniform droplets, similar to NaCl, as supported by droplet shape, uniformity, and lack of a dark continuous

https://dx.doi.org/10.1021/acs.langmuir.0c03244
Langmuir 2021, 37, 2649−2657

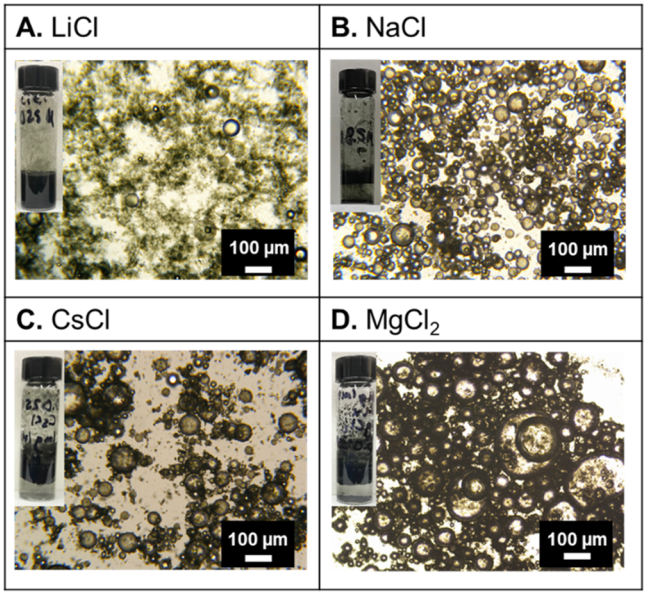

Figure 3. Optical microscopy images and photographs of 1:5 vol/vol toluene/water emulsions stabilized by 1 mg/mL $Ti_3C_2T_z$ nanosheets flocculated using 0.025 M salt concentrations of (A) LiCl, (B) NaCl, (C) CsCl, and (D) $MgCl_2$. Images were taken immediately after emulsion formation.

phase. Figure S5 shows the stability of these emulsions over 72 h, supporting that the flocculation of nanosheets with CsCl gives stable emulsions, as did the flocculation with NaCl. The difference in the formation of emulsions based on salt identity may be attributed to the different ionic radius of the cations or ionic strength (e.g., Na^+ vs Mg^{2+}). Of note, the addition of 0.025 M LiCl flocculates the $Ti_3C_2T_z$ nanosheets but does not lead to emulsion formation, as supported by the darker regions of the optical microscopy image. However, at significantly higher concentrations of LiCl (0.5 M), emulsion formation was observed (Figure S6). Computational studies support that interactions with the MXene nanosheets are cation specific;[56−59] for example, Balke and co-workers[56] and others[60,61] found that Na^+ has a higher adsorption than Li^+ and Mg^{2+}.

Capsule Formation and Characterization. Following some of our previous work with GO stabilized Pickering emulsions, we leveraged interfacial polymerization with the $Ti_3C_2T_z$-stabilized emulsions for the formation of capsules with a core of toluene and shell of polyurea and $Ti_3C_2T_z$ nanosheets. First, an oil-in-water emulsion was formed as described above, using 1 mg/mL $Ti_3C_2T_z$ nanosheets flocculated with 0.025 M NaCl and a 1:4 oil/water ratio but with hexamethylene diisocyanate (HDI) added to the toluene. Similar to the system without HDI, the resulting emulsion had uniform, distinct droplets, as verified by optical microscopy imaging (Figure 4A). An aqueous solution of ethylenediamine (EDA) was then added to the continuous aqueous phase, and the vial was swirled. Step growth polymerization between the diisocyanate and the diamine occurred at the fluid−fluid interface, encasing the $Ti_3C_2T_z$ nanosheets and forming a composite shell of nanosheets and polyurea with a core of toluene (Figure 4B). Optical microscopy images and size distribution revealed that the diameter of the emulsion droplets and capsules are similar, 10−50 μm (Figure S7).

To compare the stability of the emulsion and capsules, an alcohol challenge was performed on both samples. Briefly, ethanol was added to the HDI/toluene-in-water emulsions and to a dispersion of the capsules, followed by vigorously shaking. The addition of ethanol removes the toluene from the droplet core and thus indicates the stability of the interfacial assembly (i.e., nanosheets or polymer/nanosheet composites). As shown in Figure 4C, the addition of ethanol led to destruction of the emulsion droplets and the formation of large aggregates of $Ti_3C_2T_z$ nanosheets. In contrast, after the addition of ethanol to the capsules, the structures maintained their distinct spherical shape, though likely collapsed, as determined by optical microscopy imaging (Figure 4D). These results indicate that interfacial polymerization led to discrete, stable capsule shells permeable to ethanol and toluene.

The capsules were isolated by filtration, dried under reduced pressure, and characterized by thermogravimetric analysis

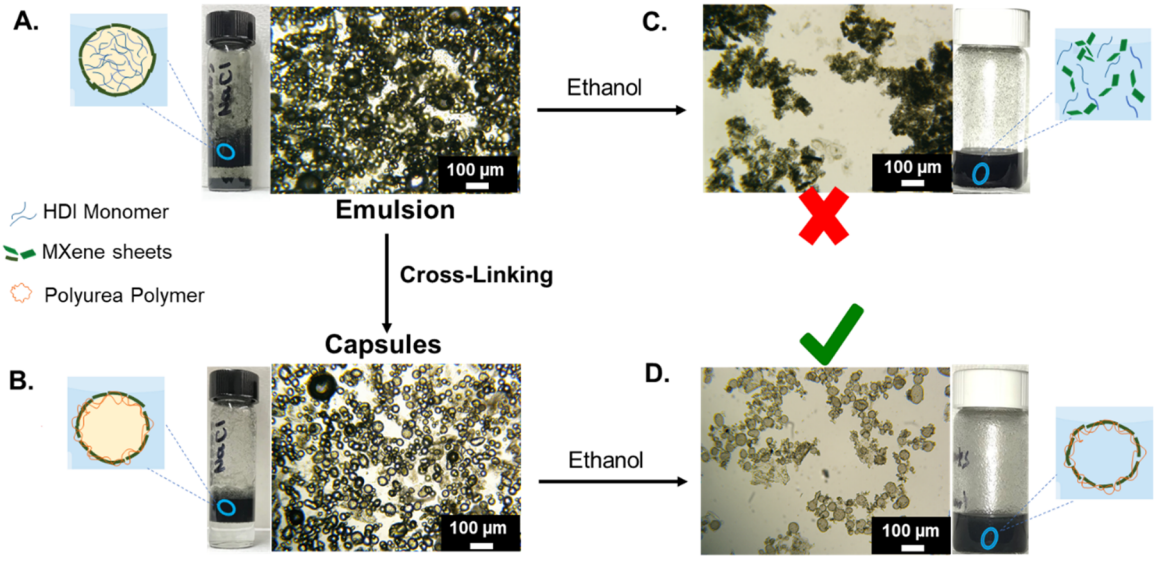

Figure 4. Capsule formation. (A) Optical microscopy image and photograph of an emulsion prepared with 1 mg/mL $Ti_3C_2T_z$ and 0.025 M NaCl. (B) Optical microscopy image and photograph of capsules after interfacial polymerization. (C, D) Optical microscopy images and photographs of an emulsion and capsules after the addition of ethanol.

https://dx.doi.org/10.1021/acs.langmuir.0c03244
Langmuir 2021, 37, 2649−2657

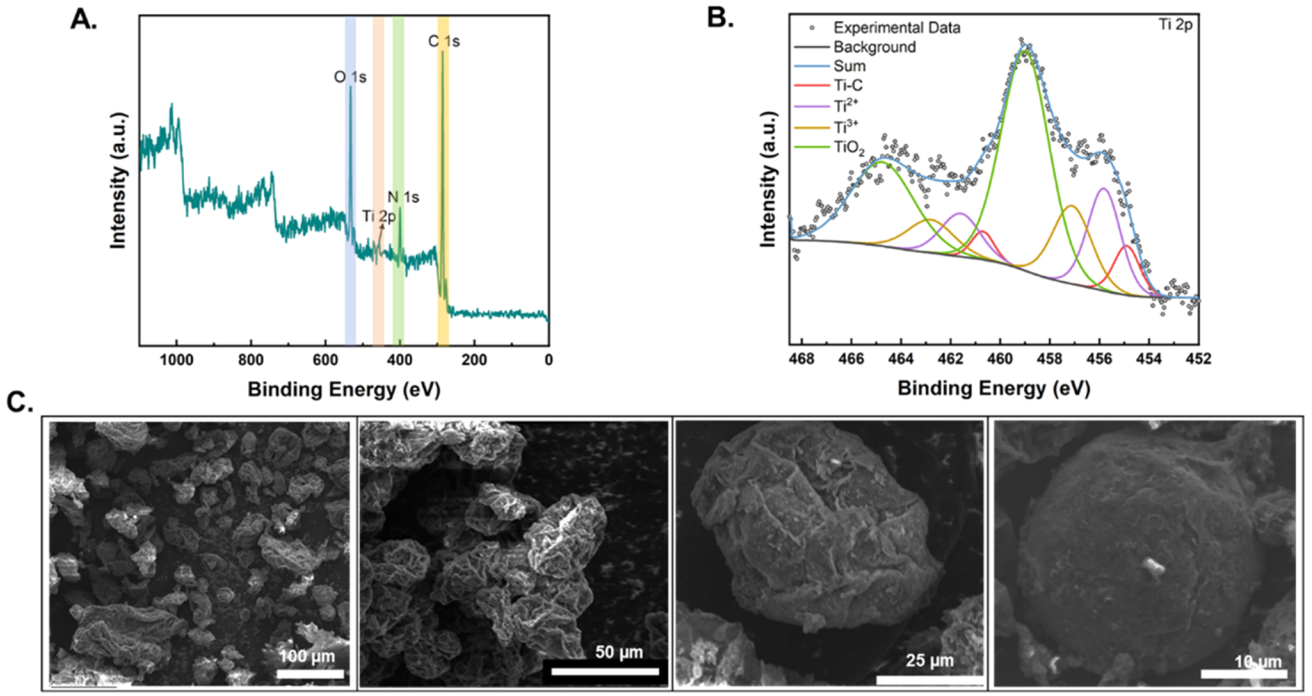

Figure 5. XPS data for capsules prepared by flocculation of $Ti_3C_2T_z$ with NaCl and interfacial polymerization: (A) survey spectrum and (B) deconvoluted high resolution Ti 2p spectrum. (C) SEM images of capsules after drying under reduced pressure.

(TGA), Fourier transform infrared (FTIR) spectroscopy, scanning electron microscopy (SEM), energy dispersive X-ray spectroscopy (EDS), and X-ray photoelectron spectroscopy (XPS). Such processing of the capsules led to the removal of the toluene core, and thus, only the capsule shell was characterized. The TGA data show weight loss attributed to the polymer (210−500 °C) with approximately 3% residual mass at 800 °C, attributed to the $Ti_3C_2T_z$ MXenes (Figure S8). The FTIR spectrum of the capsules was consistent with polyurea, showing a strong stretching frequency attributed to the carbonyl group (C═O) at 1631 cm^{-1} and a sharp low intensity stretching frequency above 3000 cm^{-1}, indicative of N−H bonds (Figure S9). The XPS survey spectrum of the capsules showed the presence of C, N, O, and Ti (Figure 5A), indicating the presence of both polymer and nanosheet. High resolution spectra for the C 1s, N 1s, and O 1s binding energies are shown in Figure S10 and that of the Ti 2p binding energy is shown in Figure 5B. The distinct Ti 2p peak was deconvoluted into Ti−C, Ti^{2+}, Ti^{3+}, and TiO_2. Among all the Ti 2p components, TiO_2 possesses the largest area; this species can be attributed to the oxidation of $Ti_3C_2T_z$ MXenes and may be due to aging of the sample. SEM images (Figure 5C) show that the morphology of the capsules at the surface is semi-spherical and wrinkled. The wrinkling may be due to the collapse of the capsule shell upon removal of toluene. The element composition of the capsules was investigated by EDS; the capsules were 54.2 wt % C, 22.0 wt % N, 21.1 wt % O, and 2.7 wt % Ti (Figure S11). This composition is consistent with the amount of MXene and polymer that is expected, assuming all monomer becomes polymer (i.e., shell is expected to be 98 wt % polymer) and indicative of the successful formation of capsules with $Ti_3C_2T_z$ embedded in the polyurea shell. In addition to the formation of capsules from $Ti_3C_2T_z$ flocculated with NaCl, capsules were prepared using CsCl as flocculant, giving similar results (Figure S12).

CONCLUSIONS

$Ti_3C_2T_z$ MXene-stabilized oil-in-water Pickering emulsions were prepared by flocculating the nanosheets with inorganic salts, adding toluene, and then agitating. Optical microscopy images showed that 0.025 M NaCl or CsCl and 1 mg/mL $Ti_3C_2T_z$ MXenes gave the most uniform droplets and best stability (at least 72 h) with all nanosheets associated with the fluid−fluid interface. The use of LiCl led to the formation of emulsions only at a significantly higher salt concentration (0.5 M), and the use of $MgCl_2$ did not lead to the formation of emulsions under the conditions tested. Capsules with a core of toluene and shell of polyurea and MXene were prepared using these Pickering emulsions as templates and interfacial polymerization of a diamine and diisocyanate. Upon the addition of ethanol, the capsules maintained their spherical shape, whereas under the same conditions, the emulsion droplets were destroyed and large aggregates of $Ti_3C_2T_z$ nanosheets formed. These data indicate that interfacial polymerization led to the formation of stable $Ti_3C_2T_z$ MXene−polymer capsule shells. The composition of the capsule shells was characterized by FTIR, TGA, XPS, and SEM-EDS, illustrating the presence of both polyurea and $Ti_3C_2T_z$ nanosheets. This approach provides cosurfactant-free MXene-stabilized Pickering emulsions and is expected to be broadly applicable to other MXene compositions and oil/water interfaces. This work expands the range of MXene−polymer composites available and paves the way for new MXene architectures using inorganic salts as flocculating agents.

ASSOCIATED CONTENT

Supporting Information

The Supporting Information is available free of charge at https://pubs.acs.org/doi/10.1021/acs.langmuir.0c03244.

ζ potential for $Ti_3C_2T_z$ MXenes; TEM images; optical microscopy images; stability time studies; MXene

https://dx.doi.org/10.1021/acs.langmuir.0c03244
Langmuir 2021, 37, 2649−2657

emulsions; thermogravimetric analysis; FTIR spectroscopy; high resolution XPS data; SEM-EDS data; SEM images (PDF)

AUTHOR INFORMATION

Corresponding Authors

Emily B. Pentzer − *Department of Materials Science and Engineering and Department of Chemistry, Texas A&M University, College Station, Texas 77843, United States;* orcid.org/0000-0001-6187-6135; Email: emilypentzer@tamu.edu

Micah J. Green − *Artie McFerrin Department of Chemical Engineering and Department of Materials Science and Engineering, Texas A&M University, College Station, Texas 77843, United States;* orcid.org/0000-0001-5691-0861; Email: micah.green@tamu.edu

Authors

Huaixuan Cao − *Artie McFerrin Department of Chemical Engineering, Texas A&M University, College Station, Texas 77843, United States;* orcid.org/0000-0003-0848-0339

Maria Escamilla − *Department of Materials Science and Engineering, Texas A&M University, College Station, Texas 77843, United States;* orcid.org/0000-0001-8450-8909

Kailash Dhondiram Arole − *Artie McFerrin Department of Chemical Engineering, Texas A&M University, College Station, Texas 77843, United States;* orcid.org/0000-0002-4516-889X

Dustin Holta − *Department of Materials Science and Engineering, Texas A&M University, College Station, Texas 77843, United States;* orcid.org/0000-0002-4641-2620

Jodie L. Lutkenhaus − *Artie McFerrin Department of Chemical Engineering, Texas A&M University, College Station, Texas 77843, United States;* orcid.org/0000-0002-2613-6016

Miladin Radovic − *Department of Materials Science and Engineering, Texas A&M University, College Station, Texas 77843, United States;* orcid.org/0000-0003-4571-2848

Complete contact information is available at: https://pubs.acs.org/10.1021/acs.langmuir.0c03244

Author Contributions

†H.C. and M.E. contributed equally

Notes

The authors declare no competing financial interest.

ACKNOWLEDGMENTS

The authors thank Texas A&M University for financial support. We would like to thank the TAMU Materials Characterization Facilities for the use of XPS, the TAMU Soft Matter Facility for use of TGA, and the TAMU Microscopy and Imaging Center for use of TEM, SEM, and EDS. We also thank Dr. Mustafa Akbulut's group and graduate student Shuhao Liu at Texas A&M University for help with the use of the zetasizer instrument. We acknowledge the help from Xiaofei Zhao in the synthesis process of MXenes.

REFERENCES

(1) Thickett, S. C.; Zetterlund, P. B. Preparation of Composite Materials by Using Graphene Oxide as a Surfactant in Ab Initio Emulsion Polymerization Systems. *ACS Macro Lett.* **2013**, *2* (7), 630−634.

(2) Shi, K.; Liu, Z.; Yang, C.; Li, X.-Y.; Sun, Y.-M.; Deng, Y.; Wang, W.; Ju, X.-J.; Xie, R.; Chu, L.-Y. Novel Biocompatible Thermoresponsive Poly(N-vinyl Caprolactam)/Clay Nanocomposite Hydrogels with Macroporous Structure and Improved Mechanical Characteristics. *ACS Appl. Mater. Interfaces* **2017**, *9* (26), 21979−21990.

(3) Brunier, B.; Sheibat-Othman, N.; Chniguir, M.; Chevalier, Y.; Bourgeat-Lami, E. Investigation of Four Different Laponite Clays as Stabilizers in Pickering Emulsion Polymerization. *Langmuir* **2016**, *32* (24), 6046−6057.

(4) Wei, P.; Luo, Q.; Edgehouse, K. J.; Hemmingsen, C. M.; Rodier, B. J.; Pentzer, E. B. 2D Particles at Fluid-Fluid Interfaces: Assembly and Templating of Hybrid Structures for Advanced Applications. *ACS Appl. Mater. Interfaces* **2018**, *10* (26), 21765−21781.

(5) Fadil, Y.; Man, S. H. C.; Jasinski, F.; Minami, H.; Thickett, S. C.; Zetterlund, P. B. Formation of homogeneous nanocomposite films at ambient temperature via miniemulsion polymerization using graphene oxide as surfactant. *J. Polym. Sci., Part A: Polym. Chem.* **2017**, *55* (14), 2289−2297.

(6) Merritt, S. M. J.; Wemyss, A. M.; Farris, S.; Patole, S.; Patias, G.; Haddleton, D. M.; Shollock, B.; Wan, C. Gas Barrier Polymer Nanocomposite Films Prepared by Graphene Oxide Encapsulated Polystyrene Microparticles. *ACS Applied Polymer Materials* **2020**, *2* (2), 725−731.

(7) Rodier, B. J.; de Leon, A.; Hemmingsen, C.; Pentzer, E. Polymerizations in oil-in-oil emulsions using 2D nanoparticle surfactants. *Polym. Chem.* **2018**, *9* (13), 1547−1550.

(8) Fadil, Y.; Dinh, L. N. M.; Yap, M. O. Y.; Kuchel, R. P.; Yao, Y.; Omura, T.; Aregueta-Robles, U. A.; Song, N.; Huang, S.; Jasinski, F.; Thickett, S. C.; Minami, H.; Agarwal, V.; Zetterlund, P. B. Ambient-Temperature Waterborne Polymer/rGO Nanocomposite Films: Effect of rGO Distribution on Electrical Conductivity. *ACS Appl. Mater. Interfaces* **2019**, *11* (51), 48450−48458.

(9) Luo, Q.; Pentzer, E. Encapsulation of Ionic Liquids for Tailored Applications. *ACS Appl. Mater. Interfaces* **2020**, *12* (5), 5169−5176.

(10) Luo, Q.; Wang, Y.; Yoo, E.; Wei, P.; Pentzer, E. Ionic Liquid-Containing Pickering Emulsions Stabilized by Graphene Oxide-Based Surfactants. *Langmuir* **2018**, *34* (34), 10114−10122.

(11) Hong, J.; Char, K.; Kim, B.-S. Hollow Capsules of Reduced Graphene Oxide Nanosheets Assembled on a Sacrificial Colloidal Particle. *J. Phys. Chem. Lett.* **2010**, *1* (24), 3442−3445.

(12) Zhang, P.; Lv, L.; Liang, Y.; Li, J.; Cheng, H.; Zhao, Y.; Qu, L. A versatile, superelastic polystyrene/graphene capsule-like framework. *J. Mater. Chem. A* **2016**, *4* (26), 10118−10123.

(13) Ali, M.; Meaney, S. P.; Giles, L. W.; Holt, P.; Majumder, M.; Tabor, R. F. Capture of Perfluorooctanoic Acid Using Oil-Filled Graphene Oxide-Silica Hybrid Capsules. *Environ. Sci. Technol.* **2020**, *54* (6), 3549−3558.

(14) Ali, M.; McCoy, T. M.; McKinnon, I. R.; Majumder, M.; Tabor, R. F. Synthesis and Characterization of Graphene Oxide-Polystyrene Composite Capsules with Aqueous Cargo via a Water-Oil-Water Multiple Emulsion Templating Route. *ACS Appl. Mater. Interfaces* **2017**, *9* (21), 18187−18198.

(15) Sohn, K.; Joo Na, Y.; Chang, H.; Roh, K.-M.; Dong Jang, H.; Huang, J. Oil absorbing graphene capsules by capillary molding. *Chem. Commun.* **2012**, *48* (48), 5968−5970.

(16) Luo, Q.; Wang, Y.; Chen, Z.; Wei, P.; Yoo, E.; Pentzer, E. Pickering Emulsion-Templated Encapsulation of Ionic Liquids for Contaminant Removal. *ACS Appl. Mater. Interfaces* **2019**, *11* (9), 9612−9620.

(17) de Leon, A.; Wei, P.; Bordera, F.; Wegierak, D.; McMillen, M.; Yan, D.; Hemmingsen, C.; Kolios, M. C.; Pentzer, E. B.; Exner, A. A. Pickering Bubbles as Dual-Modality Ultrasound and Photoacoustic Contrast Agents. *ACS Appl. Mater. Interfaces* **2020**, *12* (19), 22308−22317.

(18) Naguib, M.; Mashtalir, O.; Carle, J.; Presser, V.; Lu, J.; Hultman, L.; Gogotsi, Y.; Barsoum, M. W. Two-Dimensional Transition Metal Carbides. *ACS Nano* **2012**, *6* (2), 1322−1331.

(19) Naguib, M.; Mochalin, V. N.; Barsoum, M. W.; Gogotsi, Y. 25th Anniversary Article: MXenes: A New Family of Two-Dimensional Materials. *Adv. Mater.* **2014**, *26* (7), 992−1005.
(20) Alhabeb, M.; Maleski, K.; Anasori, B.; Lelyukh, P.; Clark, L.; Sin, S.; Gogotsi, Y. Guidelines for Synthesis and Processing of Two-Dimensional Titanium Carbide (Ti3C2Tx MXene). *Chem. Mater.* **2017**, *29* (18), 7633−7644.
(21) Sun, W.; Shah, S. A.; Chen, Y.; Tan, Z.; Gao, H.; Habib, T.; Radovic, M.; Green, M. J. Electrochemical etching of Ti2AlC to Ti2CTx (MXene) in low-concentration hydrochloric acid solution. *J. Mater. Chem. A* **2017**, *5* (41), 21663−21668.
(22) Hong Ng, V. M.; Huang, H.; Zhou, K.; Lee, P. S.; Que, W.; Xu, J. Z.; Kong, L. B. Recent progress in layered transition metal carbides and/or nitrides (MXenes) and their composites: synthesis and applications. *J. Mater. Chem. A* **2017**, *5* (7), 3039−3068.
(23) Naguib, M.; Kurtoglu, M.; Presser, V.; Lu, J.; Niu, J.; Heon, M.; Hultman, L.; Gogotsi, Y.; Barsoum, M. W. Two-Dimensional Nanocrystals Produced by Exfoliation of Ti3AlC2. *Adv. Mater.* **2011**, *23* (37), 4248−4253.
(24) Zhao, X.; Vashisth, A.; Prehn, E.; Sun, W.; Shah, S. A.; Habib, T.; Chen, Y.; Tan, Z.; Lutkenhaus, J. L.; Radovic, M.; Green, M. J. Antioxidants Unlock Shelf-Stable Ti3C2Tx (MXene) Nanosheet Dispersions. *Matter* **2019**, *1* (2), 513−526.
(25) Mashtalir, O.; Naguib, M.; Mochalin, V. N.; Dall'Agnese, Y.; Heon, M.; Barsoum, M. W.; Gogotsi, Y. Intercalation and delamination of layered carbides and carbonitrides. *Nat. Commun.* **2013**, *4* (1), 1716.
(26) Hart, J. L.; Hantanasirisakul, K.; Lang, A. C.; Anasori, B.; Pinto, D.; Pivak, Y.; van Omme, J. T.; May, S. J.; Gogotsi, Y.; Taheri, M. L. Control of MXenes' electronic properties through termination and intercalation. *Nat. Commun.* **2019**, *10* (1), 522.
(27) Siriwardane, E. M. D.; Demiroglu, I.; Sevik, C.; Çakır, D. Achieving Fast Kinetics and Enhanced Li Storage Capacity for Ti3C2O2 by Intercalation of Quinone Molecules. *ACS Applied Energy Materials* **2019**, *2* (2), 1251−1258.
(28) Luo, J.; Zhang, W.; Yuan, H.; Jin, C.; Zhang, L.; Huang, H.; Liang, C.; Xia, Y.; Zhang, J.; Gan, Y.; Tao, X. Pillared Structure Design of MXene with Ultralarge Interlayer Spacing for High-Performance Lithium-Ion Capacitors. *ACS Nano* **2017**, *11* (3), 2459−2469.
(29) Cai, Y.; Shen, J.; Ge, G.; Zhang, Y.; Jin, W.; Huang, W.; Shao, J.; Yang, J.; Dong, X. Stretchable Ti3C2Tx MXene/Carbon Nanotube Composite Based Strain Sensor with Ultrahigh Sensitivity and Tunable Sensing Range. *ACS Nano* **2018**, *12* (1), 56−62.
(30) Lukatskaya, M. R.; Mashtalir, O.; Ren, C. E.; Dall'Agnese, Y.; Rozier, P.; Taberna, P. L.; Naguib, M.; Simon, P.; Barsoum, M. W.; Gogotsi, Y. Cation Intercalation and High Volumetric Capacitance of Two-Dimensional Titanium Carbide. *Science* **2013**, *341* (6153), 1502.
(31) Ling, Z.; Ren, C. E.; Zhao, M.-Q.; Yang, J.; Giammarco, J. M.; Qiu, J.; Barsoum, M. W.; Gogotsi, Y. Flexible and conductive MXene films and nanocomposites with high capacitance. *Proc. Natl. Acad. Sci. U. S. A.* **2014**, *111* (47), 16676.
(32) Wang, X.; Shen, X.; Gao, Y.; Wang, Z.; Yu, R.; Chen, L. Atomic-Scale Recognition of Surface Structure and Intercalation Mechanism of Ti3C2X. *J. Am. Chem. Soc.* **2015**, *137* (7), 2715−2721.
(33) Wu, Z.; Shang, T.; Deng, Y.; Tao, Y.; Yang, Q.-H. The Assembly of MXenes from 2D to 3D. *Advanced Science* **2020**, *7* (7), 1903077.
(34) VahidMohammadi, A.; Mojtabavi, M.; Caffrey, N. M.; Wanunu, M.; Beidaghi, M. Assembling 2D MXenes into Highly Stable Pseudocapacitive Electrodes with High Power and Energy Densities. *Adv. Mater.* **2019**, *31* (8), 1806931.
(35) Yan, J.; Ren, C. E.; Maleski, K.; Hatter, C. B.; Anasori, B.; Urbankowski, P.; Sarycheva, A.; Gogotsi, Y. Flexible MXene/Graphene Films for Ultrafast Supercapacitors with Outstanding Volumetric Capacitance. *Adv. Funct. Mater.* **2017**, *27* (30), 1701264.
(36) Chen, C.; Boota, M.; Xie, X.; Zhao, M.; Anasori, B.; Ren, C. E.; Miao, L.; Jiang, J.; Gogotsi, Y. Charge transfer induced polymerization of EDOT confined between 2D titanium carbide layers. *J. Mater. Chem. A* **2017**, *5* (11), 5260−5265.
(37) Anasori, B.; Lukatskaya, M. R.; Gogotsi, Y. 2D metal carbides and nitrides (MXenes) for energy storage. *Nature Reviews Materials* **2017**, *2* (2), 16098.
(38) Lukatskaya, M. R.; Kota, S.; Lin, Z.; Zhao, M.-Q.; Shpigel, N.; Levi, M. D.; Halim, J.; Taberna, P.-L.; Barsoum, M. W.; Simon, P.; Gogotsi, Y. Ultra-high-rate pseudocapacitive energy storage in two-dimensional transition metal carbides. *Nature Energy* **2017**, *2* (8), 17105.
(39) Cheng, L.; Li, X.; Zhang, H.; Xiang, Q. Two-Dimensional Transition Metal MXene-Based Photocatalysts for Solar Fuel Generation. *J. Phys. Chem. Lett.* **2019**, *10* (12), 3488−3494.
(40) Seh, Z. W.; Fredrickson, K. D.; Anasori, B.; Kibsgaard, J.; Strickler, A. L.; Lukatskaya, M. R.; Gogotsi, Y.; Jaramillo, T. F.; Vojvodic, A. Two-Dimensional Molybdenum Carbide (MXene) as an Efficient Electrocatalyst for Hydrogen Evolution. *ACS Energy Letters* **2016**, *1* (3), 589−594.
(41) Shahzad, F.; Alhabeb, M.; Hatter, C. B.; Anasori, B.; Man Hong, S.; Koo, C. M.; Gogotsi, Y. Electromagnetic interference shielding with 2D transition metal carbides (MXenes). *Science* **2016**, *353* (6304), 1137.
(42) Zhang, Q.; Teng, J.; Zou, G.; Peng, Q.; Du, Q.; Jiao, T.; Xiang, J. Efficient phosphate sequestration for water purification by unique sandwich-like MXene/magnetic iron oxide nanocomposites. *Nanoscale* **2016**, *8* (13), 7085−7093.
(43) Lin, H.; Chen, Y.; Shi, J. Insights into 2D MXenes for Versatile Biomedical Applications: Current Advances and Challenges Ahead. *Advanced Science* **2018**, *5* (10), 1800518.
(44) Gao, G.; O'Mullane, A. P.; Du, A. 2D MXenes: A New Family of Promising Catalysts for the Hydrogen Evolution Reaction. *ACS Catal.* **2017**, *7* (1), 494−500.
(45) Orangi, J.; Hamade, F.; Davis, V. A.; Beidaghi, M. 3D Printing of Additive-Free 2D Ti3C2Tx (MXene) Ink for Fabrication of Micro-Supercapacitors with Ultra-High Energy Densities. *ACS Nano* **2020**, *14* (1), 640−650.
(46) Bian, R.; Lin, R.; Wang, G.; Lu, G.; Zhi, W.; Xiang, S.; Wang, T.; Clegg, P. S.; Cai, D.; Huang, W. 3D assembly of Ti3C2-MXene directed by water/oil interfaces. *Nanoscale* **2018**, *10* (8), 3621−3625.
(47) Shi, S.; Qian, B.; Wu, X.; Sun, H.; Wang, H.; Zhang, H.-B.; Yu, Z.-Z.; Russell, T. P. Self-Assembly of MXene-Surfactants at Liquid-Liquid Interfaces: From Structured Liquids to 3D Aerogels. *Angew. Chem., Int. Ed.* **2019**, *58* (50), 18171−18176.
(48) Cain, J. D.; Azizi, A.; Maleski, K.; Anasori, B.; Glazer, E. C.; Kim, P. Y.; Gogotsi, Y.; Helms, B. A.; Russell, T. P.; Zettl, A. Sculpting Liquids with Two-Dimensional Materials: The Assembly of Ti3C2Tx MXene Sheets at Liquid-Liquid Interfaces. *ACS Nano* **2019**, *13* (11), 12385−12392.
(49) Zhao, S.; Li, L.; Zhang, H.-B.; Qian, B.; Luo, J.-Q.; Deng, Z.; Shi, S.; Russell, T. P.; Yu, Z.-Z. Janus MXene nanosheets for macroscopic assemblies. *Materials Chemistry Frontiers* **2020**, *4* (3), 910−917.
(50) Ashby, N. P.; Binks, B. P. Pickering emulsions stabilised by Laponite clay particles. *Phys. Chem. Chem. Phys.* **2000**, *2* (24), 5640−5646.
(51) Deng, Y.; Shang, T.; Wu, Z.; Tao, Y.; Luo, C.; Liang, J.; Han, D.; Lyu, R.; Qi, C.; Lv, W.; Kang, F.; Yang, Q.-H. Fast Gelation of Ti3C2Tx MXene Initiated by Metal Ions. *Adv. Mater.* **2019**, *31* (43), 1902432.
(52) Yaakov, N.; Ananth Mani, K.; Felfbaum, R.; Lahat, M.; Da Costa, N.; Belausov, E.; Ment, D.; Mechrez, G. Single Cell Encapsulation via Pickering Emulsion for Biopesticide Applications. *ACS Omega* **2018**, *3* (10), 14294−14301.
(53) Gao, H.; Benitez, R.; Son, W.; Arroyave, R.; Radovic, M. Structural, physical and mechanical properties of Ti3(Al1-xSix)C2 solid solution with x = 0−1. *Mater. Sci. Eng., A* **2016**, *676*, 197−208.
(54) Shah, S. A.; Habib, T.; Gao, H.; Gao, P.; Sun, W.; Green, M. J.; Radovic, M. Template-free 3D titanium carbide (Ti3C2Tx) MXene

https://dx.doi.org/10.1021/acs.langmuir.0c03244
Langmuir 2021, 37, 2649−2657

particles crumpled by capillary forces. *Chem. Commun.* **2017**, *53* (2), 400−403.
(55) Marinova, K. G.; Alargova, R. G.; Denkov, N. D.; Velev, O. D.; Petsev, D. N.; Ivanov, I. B.; Borwankar, R. P. Charging of Oil-Water Interfaces Due to Spontaneous Adsorption of Hydroxyl Ions. *Langmuir* **1996**, *12* (8), 2045−2051.
(56) Gao, Q.; Sun, W.; Ilani-Kashkouli, P.; Tselev, A.; Kent, P. R. C.; Kabengi, N.; Naguib, M.; Alhabeb, M.; Tsai, W.-Y.; Baddorf, A. P.; Huang, J.; Jesse, S.; Gogotsi, Y.; Balke, N. Tracking ion intercalation into layered Ti3C2MXene films across length scales. *Energy Environ. Sci.* **2020**, *13* (8), 2549−2558.
(57) Ding, L.; Li, L.; Liu, Y.; Wu, Y.; Lu, Z.; Deng, J.; Wei, Y.; Caro, J.; Wang, H. Effective ion sieving with Ti3C2Tx MXene membranes for production of drinking water from seawater. *Nature Sustainability* **2020**, *3* (4), 296−302.
(58) Berdiyorov, G. R.; Mahmoud, K. A. Effect of surface termination on ion intercalation selectivity of bilayer Ti3C2T2 (T = F, O and OH) MXene. *Appl. Surf. Sci.* **2017**, *416*, 725−730.
(59) Muckley, E. S.; Naguib, M.; Wang, H.-W.; Vlcek, L.; Osti, N. C.; Sacci, R. L.; Sang, X.; Unocic, R. R.; Xie, Y.; Tyagi, M.; Mamontov, E.; Page, K. L.; Kent, P. R. C.; Nanda, J.; Ivanov, I. N. Multimodality of Structural, Electrical, and Gravimetric Responses of Intercalated MXenes to Water. *ACS Nano* **2017**, *11* (11), 11118−11126.
(60) Eames, C.; Islam, M. S. Ion Intercalation into Two-Dimensional Transition-Metal Carbides: Global Screening for New High-Capacity Battery Materials. *J. Am. Chem. Soc.* **2014**, *136* (46), 16270−16276.
(61) Ren, C. E.; Hatzell, K. B.; Alhabeb, M.; Ling, Z.; Mahmoud, K. A.; Gogotsi, Y. Charge- and Size-Selective Ion Sieving Through Ti3C2Tx MXene Membranes. *J. Phys. Chem. Lett.* **2015**, *6* (20), 4026−4031.

https://dx.doi.org/10.1021/acs.langmuir.0c03244
Langmuir 2021, 37, 2649−2657